Monthly Notices of the ROYAL ASTRONOMICAL SOCIETY

MNRAS **545,** 1–8 (2026) https://doi.org/10.1093/mnras/staf2112
Advance Access publication 2025 November 27

Simulating the stellar bycatch: constraining the prevalence of extraterrestrial transmitters within radio SETI surveys

Louisa A. Mason [1★] Michael A. Garrett[1,2,3] and Andrew P. V. Siemion[1,3,4,5,6]

[1]*Jodrell Bank Centre for Astrophysics, Department of Physics and Astronomy, University of Manchester, Alan Turing Building, Oxford Road, Manchester M13 9PL, UK*
[2]*Leiden Observatory, Leiden University, PO Box 9513, NL-2300 RA Leiden, the Netherlands*
[3]*Institute of Space Sciences and Astronomy, University of Malta, Msida MSD 2080, Malta*
[4]*Astrophysics Sub-Department, Department of Physics, University of Oxford, Denys Wilkinson Building, Keble Road, Oxford OX1 3RH, UK*
[5]*SETI Institute, 339 Bernardo Avenue, Suite 200, Mountain View, CA 94043, USA*
[6]*Berkeley SETI Research Center, University of California, Berkeley, CA 94720, USA*

Accepted 2025 November 21. Received 2025 November 7; in original form 2025 August 20

ABSTRACT

Searches for radio technosignatures place constraints on the prevalence of extraterrestrial transmitters in our Galaxy and beyond. It is important to account for the complete stellar population captured within a radio telescope's field of view, or stellar 'bycatch'. In recent years, catalogues from ESA's *Gaia* mission have enabled the search for extraterrestrial intelligence (SETI) surveys to place tighter limits on extraterrestrial transmitter statistics. However, *Gaia* remains restricted by magnitude limits, astrometric uncertainty at large distances, and confusion in crowded regions. To address these limitations, we investigate the use of the Besançon Galactic model to simulate the statistical underlying stellar population to derive more realistic constraints on the occurrence of extraterrestrial transmitters. We apply this method to Breakthrough Listen's Enriquez/Price survey, modelling 6182 364 stellar objects within 1229 individual pointings and extending the search out to distances $\leq$25 kpc. We place limits on the prevalence of high-duty-cycle transmitters within 2.5 kpc, suggesting $\leq(0.000995 \pm 0.000002)$ per cent of stellar systems contain such a transmitter (for near-zero drift rates and $\mathrm{EIRP_{min}} \gtrsim 5 \times 10^{16}$ W). In support of broader adoption, we provide a simple calculator tool that enables other researchers to incorporate this approach into their own SETI analyses. Our results enable a more complete statistical estimation of the number and stellar type of systems probed, thereby strengthening constraints on technosignature prevalence and guiding the analysis of future SETI efforts. We also conclude that SETI surveys are, in fact, much less biased by anthropocentric assumptions than is often suggested.

Key words: extraterrestrial intelligence – radio lines: stars – submillimetre: stars.

1 INTRODUCTION

The search for extraterrestrial intelligence (SETI) – whether for intentional beacons, accidental leakage, or relic signals from extinct civilizations – spans a vast and complex parameter space. This includes dimensions such as position on the sky, observing frequency, total bandwidth, spectral resolution, temporal cadence, signal modulation, and sensitivity, as discussed by J. T. Wright, S. Kanodia & E. Lubar (2018). SETI surveys aim to reduce the volume of unsearched multidimensional parameter space to tighten the bounds on the prevalence of extraterrestrial transmitters.

Narrow-band single-dish SETI surveys typically search for signals across a broad range of Doppler drift rates (e.g. ± 4 Hz s^{-1}) and possess a field of view at 1 GHz that spans several arcminutes. Each pointing thus encompasses a significant number of background (and occasionally foreground) celestial objects (N_*) which are passively included in the analysis of the integrated power spectrum. As a result, these surveys are sensitive not only to signals originating from the nominal target star, but also to potential transmitters distributed across the full field of view. Quantifying this 'stellar bycatch' – the incidental population of stars within the telescope beam – enables more realistic constraints to be placed on the prevalence of extraterrestrial transmitters probed by SETI surveys (see B. S. Wlodarczyk-Sroka, M. A. Garrett & A. P. V. Siemion 2020).

ESA's *Gaia* mission and its associated astrometric catalogue have enabled better estimates of the Galactic stellar bycatch for the original Breakthrough Listen surveys by J. E. Enriquez et al. (2017) and D. C. Price et al. (2020) (see B. S. Wlodarczyk-Sroka et al. 2020). This methodology has since been adopted by other studies, including those by J.-L. Margot et al. (2023), O. A. Johnson et al. (2023), and L. A. Mason et al. (2025). The inclusion of the stellar bycatch increases the total population of stars surveyed within a given pointing direction and observational time frame.

However, the latest *Gaia* data release includes only 1.8 billion Galactic objects (Gaia Collaboration 2023) and remains limited by magnitude limits, astrometric uncertainties, and confusion in densely populated regions. Catalogues derived from *Gaia*, such as those by

★ E-mail: louisa.mason@manchester.ac.uk

C. A. L. Bailer-Jones et al. (2021), represent a lower bound on the true stellar bycatch encountered in SETI surveys.

By utilizing Galactic stellar population synthesis models, we can not only predict the number distribution of stars as a function of distance for a particular cut through the Milky Way, but also yield the range of stellar classes that a typical survey passively includes. Even strictly 'targeted' single-dish SETI surveys nominally focused on specific stellar types (such as nearby main-sequence stars) invariably encompass a much broader array of spectral types through their incidental stellar bycatch. Without accounting for this broader context, we risk underestimating the true extent and scientific reach of SETI survey efforts.

In this paper, we use the Besançon Galactic model (BGM) to simulate stars within the field of view of SETI surveys in order to place better limits on the prevalence of extraterrestrial transmitters in the Milky Way. In Section 2, we discuss the limitations of using *Gaia* alone to estimate the stellar bycatch population and briefly outline the BGM's simulation method. In Section 3, we utilize the BGM to simulate the stellar population associated with the D. C. Price et al. (2020) survey and compare the limits on prevalence and stellar population properties calculated against previous studies utilizing *Gaia* by B. S. Wlodarczyk-Sroka et al. (2020). In Section 4, we provide a public domain calculator that estimates the stellar bycatch as a function of pointing position and field of view. In Section 5, we present our conclusions and evaluate the significance of employing simulations to estimate the stellar bycatch for future SETI surveys.

2 MODELLING THE MILKY WAY

2.1 Limitations of *Gaia*

ESA's *Gaia* mission has transformed our understanding of the Milky Way by providing astrometric measurements for over a billion stellar objects. However, like all observational data sets, its completeness and reliability are subject to important limitations.

The mission achieves high completeness for stars with apparent magnitudes in the range $12 < G < 17$, and can extend to $G \sim 20$ in regions of low stellar density. In contrast, heavily crowded fields with more than 400 000 stars per square degree see completeness drop to $G \sim 18$ (X. Luri et al. 2018). Distance estimates are also affected by parallax uncertainties; for sources with a fractional parallax error $f > 0.2$, geometric distance estimates such as those provided by C. A. L. Bailer-Jones et al. (2021) are preferred. In the cases of large or negative fractional parallax errors, inferred distances are dominated by modelling prior errors. This limits reliable distance estimation within the *Gaia* catalogue (where $0 < f < 1$) to within 10 kpc.

The classification of stellar types in *Gaia* is typically inferred from photometric colour, using the difference $G_{\rm BP} - G_{\rm RP}$. However, in crowded regions or for faint sources, background contamination and confusion – particularly from unresolved binaries – can significantly degrade the accuracy of spectral classification (F. Arenou et al. 2018). Distinguishing between nearby main-sequence stars and white dwarfs, for instance, is often problematic in these regimes.

To mitigate these issues, stringent quality filters are applied to extract clean stellar samples. Yet this comes at a high cost: only about 30 per cent of objects in *Gaia* Data Release 2 (DR2) pass the recommended contamination filters (F. Arenou et al. 2018). As a result, while *Gaia* provides an invaluable foundation for stellar population studies, it offers only a lower limit on the true number of stars intercepted by wide-field SETI observations.

2.2 The Besançon Galactic model

The BGM (A. C. Robin et al. 2004; O. Bienaymé, J. Leca & A. C. Robin 2018) is a dynamical self-consistent model of the Milky Way. The model is used across astrophysics research, including studies of Galactic structure, stellar populations (in particular for low-mass stars), extinction mapping, and microlensing predictions (e.g. C. Reylé et al. 2009; M. A. Czekaj et al. 2014; D. Specht et al. 2020; T. Ravinet et al. 2022). In the context of stellar population synthesis, the BGM has proven especially valuable for modelling star counts, kinematics, and photometric distributions across a range of sky directions.

The model divides the Galaxy into four subcomponents: the thin disc, the thick disc, the bulge, and stellar halo. The thin disc has been divided into seven subpopulations based on age, each modelled by an Einasto relation describing the 3D density distribution (J. Einasto 1979). The thick disc is modelled by two isochrones, due to the 2 Gyr long star formation period. The halo can be considered a homogeneous population of stars with a short star-forming period. A Salpeter initial mass function (IMF) is assumed for the bulge, despite the difficulty in constraining low-mass stars within the bulge (due to crowding).

The stellar densities are constrained by the Galactic potential (Poisson equation), velocity dispersion of each subcomponent (based on the age–velocity dispersion relation), and the Galactic rotation curve (to estimate the scale heights/axis ratio of each subpopulation). The model is initially based on the stellar neighbourhood, before scaling outwards to the full extent of the Milky Way.

The population of stars within each subcomponent of the Galaxy can be estimated, given

$$N_* = \int \Phi(m)\,{\rm d}m \int \Psi(t)\,{\rm d}t, \tag{1}$$

where $\Phi(m)$ is the initial mass function and $\Psi(t)$ is the star formation rate (M. Haywood 1994). For a number of stars per age and mass interval, the BGM uses evolutionary tracks to evaluate further stellar parameters. If interpolating along the evolutionary tracks results in a solution, the star's luminosity L, surface gravity g, and effective temperature $T_{\rm eff}$ are assigned; if not, the star is considered a 'stellar remnant'. For stars with assigned L, g, and $T_{\rm eff}$, the photometric colour is estimated using an atmosphere model (BaSeL – Basel Stellar Library). Reddening is considered using 3D extinction models to estimate the apparent magnitude of stars based on the line of sight through the Galaxy.

The BGM has been constrained against several surveys: *Hipparcos*/Tycho for the local vicinity/self-consistent densities, *Gaia*, RAVE (RAdial Velocity Experiment), and 2MASS (Two Micron All-Sky Surve) for the outer disc scales [see M. A. Czekaj et al. (2014), A. C. Robin et al. (2022), and B. Déforêt et al. (2024) for a sample of the extensive updates to this Galactic synthesis model from observational data sets]. White dwarfs are modelled from cooling tracks, and classified into three broad populations: hydrogen-rich white dwarfs (labelled DA), helium-rich white dwarfs (labelled DB), and continuous spectrum white dwarfs (labelled DC). Asymptotic giant branch (AGB) stars are added empirically, but brown dwarfs are not modelled by the BGM.

The BGM models the stellar population down to the hydrogen burning limit of red dwarfs ($M > 0.12\ {\rm M}_\odot$). However, the assumed IMFs are poorly constrained for low-mass stars and likely contaminated by galaxies for $V > 22$ (A. C. Robin et al. 2004). Improved 3D extinction maps remain limited for lines of sight of high density

and insufficient completeness, such as within the Galactic Centre and spiral arm tangents (D. J. Marshall et al. 2006).

3 APPLICATION TO CURRENT SETI SURVEYS

3.1 The Enriquez/Price survey

J. E. Enriquez et al. (2017) conducted a survey of 692 stars using the 100-m Robert C. Byrd Green Bank Telescope (GBT) at *L* band. The target sample was derived from the list proposed by H. Isaacson et al. (2017) for the Breakthrough Listen initiative, which included the 60 closest stars, a range of *Hipparcos* stars across various spectral classes, and a selection of exotic objects (e.g. white dwarfs, neutron stars, and asteroids). D. C. Price et al. (2020) extended this survey by observing 1327 stars from Isaacson's list, again using the GBT at *L* band (1.10–1.90 GHz) and *S* band (1.80–2.80 GHz), as well as the 64-m CSIRO Parkes Telescope at 10 cm (2.60–3.45 GHz).

Building on these efforts, B. S. Wlodarczyk-Sroka et al. (2020) refined the constraints on the prevalence of extraterrestrial transmitters by incorporating additional stars within the field of view [defined by the full width at half-maximum (FWHM) of the telescope beam] provided by *Gaia* DR2. This furnished a total of 288 315 stars across the 1327 observed pointings: 251 983 at *L* band, 172 572 at *S* band, and 72 030 at 10 cm.

We have extended the B. S. Wlodarczyk-Sroka et al. (2020) approach by simulating the stellar bycatch population using the BGM. For 1229 unique pointings from Price's survey, a population of stars was generated without restrictions on the magnitude of stars for distances up to 25 kpc. Two fields located along $b \approx 0^\circ$ towards the Galactic Centre were too dense to simulate using the web portal for the BGM, taking too long to run, and so were excluded from our analysis.

Fig. 1 illustrates the simulated stellar bycatch for a single pointing – towards the target star *Gaia* DR2 5278042880077383040 – generated using the BGM, and compared against stars observed by *Gaia*.

Our simulated stellar sample, derived from the 1229 pointings, includes a total of 6182 364 stars. This represents a substantial increase compared to the 288 315 stars identified using *Gaia* in the study by B. S. Wlodarczyk-Sroka et al. (2020). We utilize the simulated BGM sample to challenge the limitations of using observational catalogues to estimate the stellar bycatch and prevalence of technosignatures.

3.2 Extending the stellar bycatch

For each simulated star, we calculate the minimum detectable equivalent isotropic radiated power ($\mathrm{EIRP_{min}}$) based on the distance to the star and position with respect to the telescope's field of view. We restrict the field of view to the FWHM of the telescope beam, represented by a Gaussian response.

The $\mathrm{EIRP_{min}}$ values reported here correspond to the maximum sensitivity achieved when searching for signals with near-zero drift rates. For drift rates exceeding ± 0.15 Hz s^{-1}, narrow-band signals can become smeared across multiple frequency channels – depending on the survey's spectral resolution and integration time – leading to a reduction in sensitivity to such signals (J.-L. Margot et al. 2021). Neither the original analysis by D. C. Price et al. (2020) nor the subsequent reanalysis by B. S. Wlodarczyk-Sroka et al. (2020) account for this effect. To enable a direct comparison with these earlier studies, we have similarly not applied a correction for Doppler smearing in the $\mathrm{EIRP_{min}}$ or Continuous Waveform Transmitter Figure of Merit (CWTFM) values presented here. However, we do note that future surveys should correct their results for this effect, as detailed in J.-L. Margot et al. (2021).

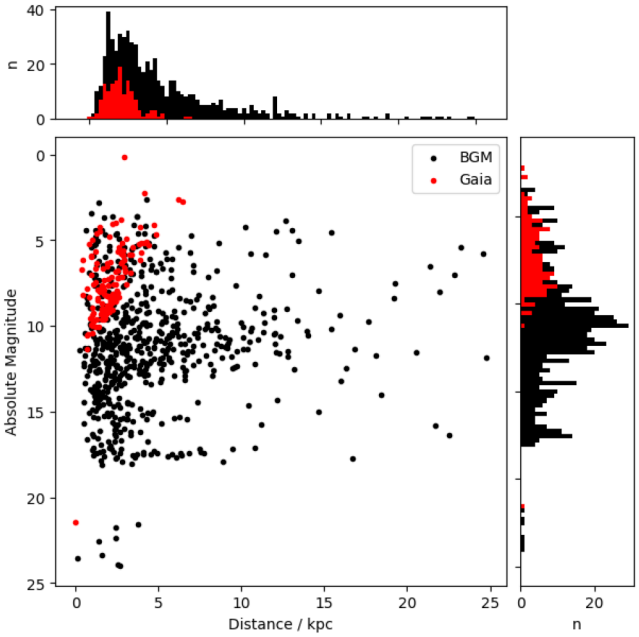

Figure 1. The sample of stars within a single pointing (in the direction of $l = 276.05^\circ$, $b = -14.4^\circ$) simulated by the BGM (in black) compared to the sample of stars from *Gaia* with accurate parallax measurements (in red). We compare the distribution in absolute magnitudes (right) and the distribution of distances (top). The BGM can be used to expand the stellar sample beyond the observational magnitude limitations of *Gaia*, as well as considering the full breadth of the Milky Way.

Table 1. For increasing shells of $\mathrm{EIRP_{min}}$, the stellar bycatch population simulated by the BGM (N_B) and observed by *Gaia* (N_G) are compared, and the figure of merit, CWTFM, is estimated for each BGM population. The upper distance limits (d) have been calculated for a star within the centre of the beam (no offset correction applied). The stellar bycatch observed by *Gaia* has been subject to cuts based on fractional parallax uncertainty and restricted to distances <10 kpc (see B. S. Wlodarczyk-Sroka et al. 2020). The BGM increases the stellar bycatch population for $\mathrm{EIRP_{min}} > 10^{15}$ W.

	$\mathrm{EIRP_{min}}$ (W)	d (pc)	N_B	N_G	CWTFM
GBT	10^{14}	290	1828	2599	3.56
	10^{15}	930	36 071	25 192	1.80
	10^{16}	2940	367 616	147 976	1.77
	10^{17}	9310	3091 788	246 245	2.10
	10^{18}	25 000	5115 832	246 492	12.71
Parkes	10^{14}	160	98	82	181.57
	10^{15}	500	2019	695	88.13
	10^{16}	1600	26 613	5225	66.86
	10^{17}	5050	267 747	30 434	66.46
	10^{18}	16 000	1178 528	40 592	150.99

Table 1 presents the number of stars simulated by the BGM and observed by *Gaia* for increasing shells of $\mathrm{EIRP_{min}}$, as well as the CWTFM. CWFTM is a widely used figure of merit in evaluating the effectiveness of radio SETI surveys, and depends on the $\mathrm{EIRP_{min}}$, the fractional bandwidth ($\nu_\mathrm{rel} = \Delta\nu/\nu_0$), and the total number of stars observed (N_*). Following J. E. Enriquez et al. (2017) and D. C. Price

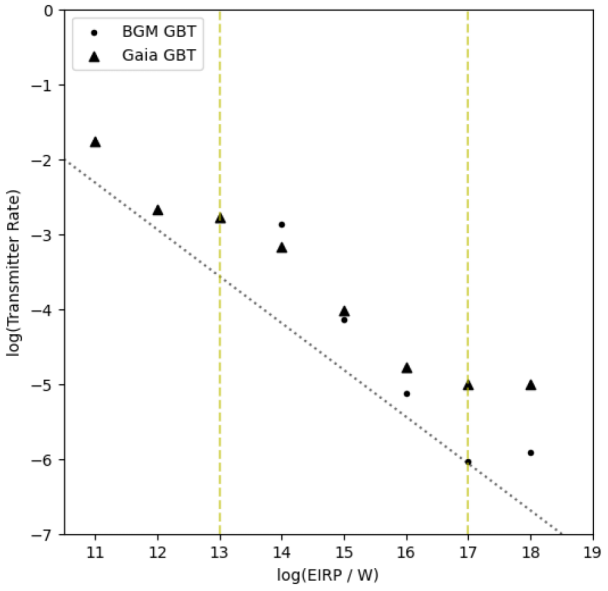

Figure 2. For GBT *L*-band and *S*-band observations, we plot a comparison of the $\mathrm{EIRP_{min}}$ and transmitter rate determined from the sample of stars up to 25 kpc using the BGM and up to 10 kpc from *Gaia* (B. S. Wlodarczyk-Sroka et al. 2020), for shells of increasing $\mathrm{EIRP_{min}}$. We plot the dashed vertical lines as a reference to a transmitter with $\mathrm{EIRP_{min}}$ equivalent to Arecibo (10^{13} W), and a transmitter with equivalent power to a Kardashev Type I civilization (10^{17} W). This work to extend the stellar bycatch using the BGM challenges the current limits in survey sensitivity and scope, represented in a grey dashed line, referred to as 'terra incognito' (M. A. Garrett & A. P. V. Siemion 2023).

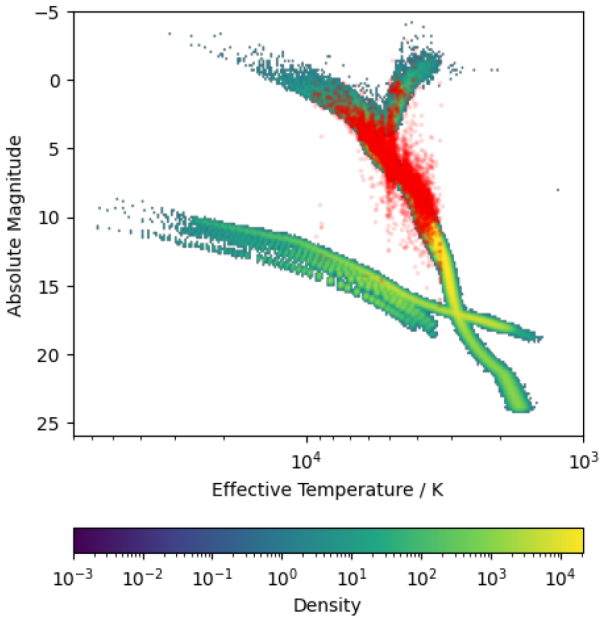

Figure 3. HR diagram comparing the BGM-simulated stellar population (background) with the subset of *Gaia* sources (superimposed in red) for which reliable effective temperatures and absolute magnitudes are available. The *Gaia* sample is restricted to within 1 kpc due to parallax accuracy, and most white dwarfs lack reliable temperature estimates. Utilizing the BGM enables consideration of the complete breadth of stellar types captured within the bycatch population, including bright main-sequence stars and minimal confusion between faint main sequence and white dwarfs.

et al. (2020), the CWTFM can be expressed as

$$\mathrm{CWTFM} = \zeta_{\mathrm{A0}} \frac{\mathrm{EIRP_{min}}}{N_* \, \nu_{\mathrm{rel}}}. \tag{2}$$

Here, ζ_{A0} is a normalization constant defined such that CWTFM = 1 corresponds to a benchmark survey: sensitivity to an Arecibo-class transmitter over 1000 stars and a fractional bandwidth of 0.5.

The application of the BGM improves the stellar bycatch population – and in turn, the CWFTM – for $\mathrm{EIRP_{min}} \geq 10^{15}$ W. By leveraging the BGM, we are able to account for a much broader stellar population, thereby extending the searchable parameter space to include potential high-power technosignatures originating from across the Milky Way.

Considering how increasing the stellar bycatch improves the $\mathrm{EIRP_{min}}$–transmitter rate parameter space, we plot Fig. 2 for GBT's $\mathrm{EIRP_{min}}$ shells. Beyond 100 pc, application of the BGM improves the transmitter rate against increasing shells of $\mathrm{EIRP_{min}}$; simulating the stellar bycatch population beyond magnitude thresholds challenges the limits of 'terra incognito' (M. A. Garrett & A. P. V. Siemion 2023) and the current searched parameter space, in terms of volume of sky searched and the sensitivity depth.

The BGM provides a powerful framework for estimating the underlying stellar population and for simulating the total stellar bycatch missed by *Gaia*. However, we note that within ∼100 pc, the BGM simulates fewer stars along the 1229 pointings than those detected by *Gaia* (see Fig. 2). Consequently, we underestimate the number of stars probed by the SETI surveys considered here for transmissions with $\mathrm{EIRP_{min}} \leq 10^{14}$ W. From these results, it looks as though the BGM underestimates the number of stars simulated on these very limited spatial scales by a factor of ∼30 per cent. We also note that, when comparing against B. S. Wlodarczyk-Sroka et al. (2020), the population of stars with $\mathrm{EIRP_{min}} \leq 10^{14}$ W contains the targets from the Enriquez/Price survey.

Beyond this range, however, the BGM provides a significantly more complete representation of the underlying stellar population, including far-field stellar objects that might otherwise be filtered out of observational catalogues due to significant astrometric uncertainties. It is therefore the preferred tool for extending bycatch estimates to larger Galactic volumes.

3.3 Diversity beyond observational magnitude limits

Galactic modelling also allows us to explore the true statistical diversity of stellar types sampled in the Enriquez/Price surveys. By plotting effective temperature against absolute magnitude in a Hertzsprung–Russell (HR) diagram (Fig. 3), we can examine the physical properties of the stellar populations simulated by the BGM. The simulation extends coverage across both extremes of the main sequence and reveals a rich population of white dwarfs. We can avoid photometric confusion in spectral classification with *Gaia* (F. Arenou et al. 2018), placing clear cuts between faint main-sequence stars and white dwarfs using the simulated bycatch.

To assess how this spectral diversity varies spatially, we analyse the distribution of stellar types as a function of Galactic latitude in Fig. 4. As expected, the greatest diversity and density of stellar types is found in the Galactic plane. However, the overall ratio of spectral types remains broadly consistent across latitudes. Restricting the sample of pointings to Galactic latitudes within ±5° and Galactic longitudes within ±5° of the Galactic Centre in Fig. 5, we provide further support, on grounds of stellar density and diversity, for continuing technosignature searches toward the inner Galaxy, particularly the Galactic Centre (V. Gajjar et al. 2021). While we note that this region

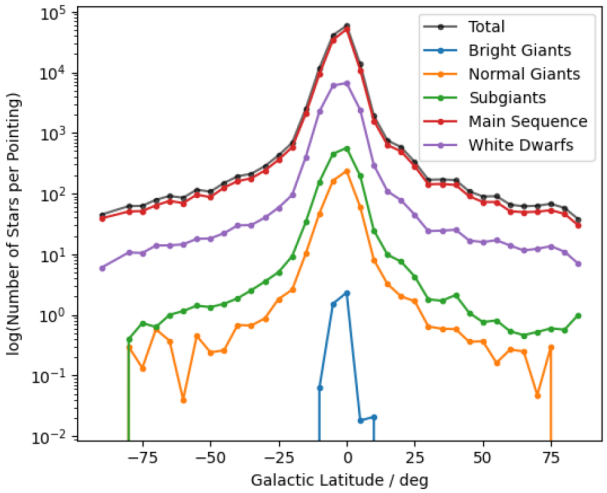

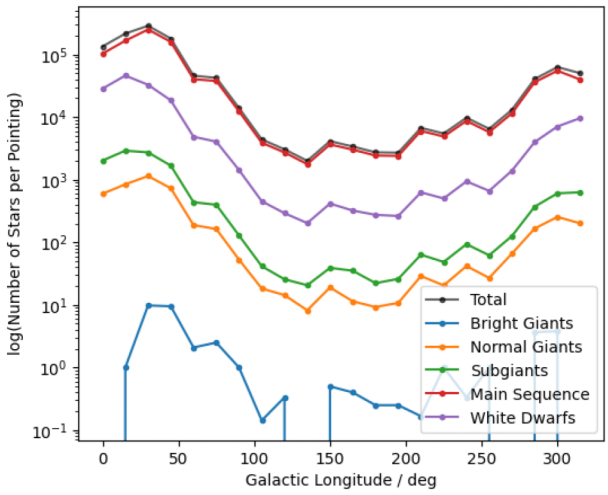

Figure 4. The distribution of stellar spectral types as a function of Galactic latitude for BGM simulations of the 1229 pointing positions. While the overall diversity peaks near the Galactic plane as expected, the relative proportions of stellar types remain broadly stable across all latitudes.

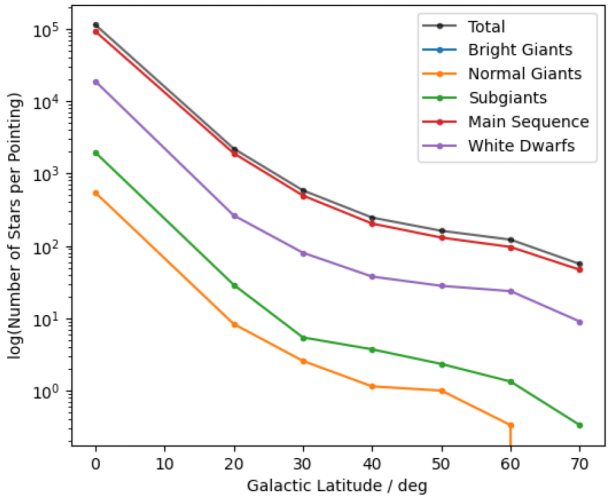

Figure 5. The distribution of stellar spectral types in relation to the Galactic plane. Upper panel: The number of stars per pointing per spectral type for $b < |5^\circ|$. Lower panel: The number of stars per pointing per spectral type for $l < |5^\circ|$. Both panels highlight the opportunistic bycatch towards the Galactic Centre for SETI endeavours.

may not be the most conducive environment for the development and sustainability of life, it remains probabilistically opportunistic for future SETI endeavours.

This modelling also highlights the diverse range of stellar types that are inadvertently included in single-dish SETI observations. Even when surveys are designed to focus on specific stellar classes, such as nearby G-type main-sequence stars, they inevitably include a broader array of stellar types as a by-product. As a result, single-dish SETI surveys, regardless of their specific targets, implicitly impose constraints on a wide variety of stellar types, including those not specifically aimed at by the principal investigator. Given the Galaxy's environmental diversity and the limited understanding of the conditions under which technological civilizations might arise, it is important to recognize these implications and consider the valuable constraints that SETI surveys inherently impose on a wide spectrum of stellar hosts. Using the BGM to estimate the stellar bycatch in SETI surveys allows us to explicitly assess and constrain the prevalence of extraterrestrial transmitters across a diverse range of stellar types.

3.4 Estimating the prevalence of ETI

A key goal of SETI surveys is to assess what their null detection results imply about the prevalence of extraterrestrial intelligence (ETI) within the Galaxy. When considering the detection of a technosignature as an independent event, and given the large number of stars encompassed within each pointing, the probability distribution of transmitter detections can be modelled as a Poisson process (C. Choza et al. 2024).

For a Poisson-distributed random variable, the probability of observing k events, given an expected mean rate λ, is given by

$$P(k|\lambda) = \frac{\lambda^k \, \mathrm{e}^{-\lambda}}{k!}.$$

In the case of a null detection ($k = 0$), this simplifies to

$$P(0|\lambda) = \mathrm{e}^{-\lambda}.$$

To set an upper bound on λ at a given confidence level C, we require

$$P(k \leq 0|\lambda_{\mathrm{upper}}) = \mathrm{e}^{-\lambda_{\mathrm{upper}}} = 1 - C.$$

Rearranging gives

$$\lambda_{\mathrm{upper}} = -\ln(1 - C).$$

For the commonly used 95 per cent confidence interval, $C = 0.95$, and thus

$$\lambda_{\mathrm{upper}} \approx -\ln(0.05) \approx 3.$$

This is the well-known 'rule of three' which allows us to estimate the upper bound of the mean detection rate (N. Gehrels 1986) as

$$\lambda \approx \frac{3}{n},$$

where n is the number of independent target stars surveyed (see J.-L. Margot et al. 2023 for alternative binomial derivation).

Applying this to our data set, we find no evidence for continuous, high-duty-cycle transmitters within the stellar bycatch of the 1229 unique pointings analysed. For distances up to 2.5 kpc, we simulate $n = 301\,472 \pm 549$ stars, leading to an estimated prevalence of such

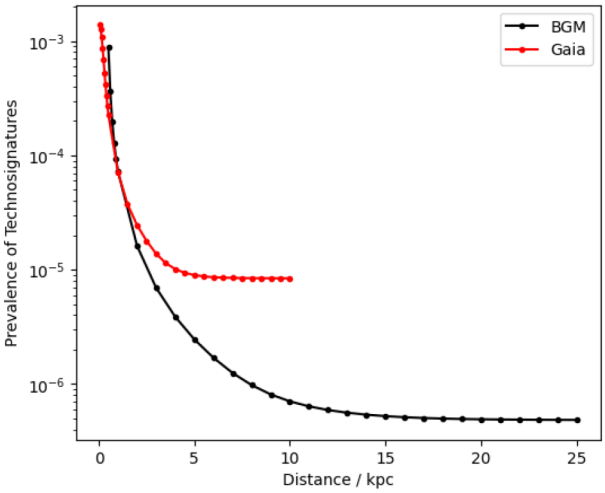

Figure 6. Estimates of the prevalence of transmitters within the Milky Way, based on the upper bound of the 95 per cent confidence interval, assuming Poisson statistics for the detection of a technosignature and a continuous high-duty-cycle transmitter. By simulating the stellar bycatch, we vastly improve the stellar bycatch population and restrict the prevalence estimated using *Gaia* beyond 2.5 kpc.

transmitters of

$$f_{\rm tx} \leq \frac{3}{n} \approx (0.000995 \pm 0.000002)\,\text{per cent},$$

for transmitters with $\text{EIRP}_{\rm min} \gtrsim 5 \times 10^{16}$ W.

By extending this analysis to concentric shells out to 25 kpc in Fig. 6, we estimate the prevalence of high-duty-cycle extraterrestrial transmitters at increasing Galactic radii. Importantly, our simulations of the stellar bycatch population provide a significantly more constrained estimate of transmitter prevalence beyond 2.5 kpc than previous *Gaia*-based approaches, while accounting for a broad range of stellar spectral types (see Appendix A).

4 APPLICATION TO FUTURE SETI SURVEYS

For the ease of application to future SETI surveys, we have developed a simple calculator to run simulations via the BGM's web service.[1] The user runs the simulation, via the BGM web portal,[2] by providing a pointing direction (in right ascension and declination) and a telescope field of view (we chose to use the FWHM for the field of view but other values are possible) for simulations that generate $\leq$2 GB. There is a time delay between job submission and completion, depending on the line of sight for the pointing and the population size to be synthesized.

The BGM simulates the stellar population for a rectangular solid angle (in deg^2), and our calculator then filters this down to only include stars with the radial field of view requested by the user. The BGM produces two output files: one containing the main stellar characteristics and another header file that records the parameters used for the simulation. The calculator extracts key stellar properties from the results (in ASCII format), including position, magnitude and colour, age, mass, effective temperature, and spectral classification. An example of this is shown in Table 2. The $\text{EIRP}_{\rm min}$ for each star is estimated given the inputted telescope's system equivalent flux density, spectral resolution, signal-to-noise ratio (SNR) threshold, and integration time. With a dechirping efficiency specified by the user, we consider the potential Doppler smearing (J.-L. Margot et al. 2021) as a result of searching at high drift rates and correct the $\text{EIRP}_{\rm min}$ for the maximum sensitivity loss. The calculator will generate a plot of the stellar bycatch population captured within the field of view (see Fig. 7 for an example), and highlights the diversity of spectral classes and luminosity types captured per pointing.

Generating a population of stars without limitations on magnitude and within 25 kpc, the calculator subdivides the bycatch population depending on their $\text{EIRP}_{\rm min}$. The $\text{EIRP}_{\rm min}$ has been corrected for the telescope's response, assuming a 2D Gaussian profile across the FWHM of the beamwidth for a single-dish telescope. The calculator generates a table for increasing $\text{EIRP}_{\rm min}$ shells of the estimated transmitter rate, based on the number of stars and the fractional bandwidth, and plots the bycatch sample in $\text{EIRP}_{\rm min}$–transmitter rate parameter space.

The calculator then subdivides the bycatch population by luminosity class and spectral type, and estimates the prevalence per stellar class for shells of increasing distance, up to 10 kpc (similar to Table A1). The breadth of diversity captured within the sample can be visually represented through the HR diagram for the stellar bycatch population simulated. Finally, the calculator estimates the prevalence of technosignatures based on the upper bound of the 95 per cent confidence interval, assuming Poisson statistics for the detection of a technosignature and a continuous high-duty-cycle transmitter (generating a plot similar to Fig. 6).

5 CONCLUSION

This paper builds on the approach of B. S. Wlodarczyk-Sroka et al. (2020) by emphasizing the importance of including the stellar bycatch for targeted radio SETI observations. By simulating stars within the field of view using the BGM, we can overcome the observational limitations of *Gaia* and improve upon statistical estimates of the prevalence of extraterrestrial transmitters across a broader stellar population, including lines of sight susceptible to confusion and crowding.

We demonstrate the use of the BGM approach through reanalysis of the Enriquez and Price surveys, simulating a sample of 6182 364 stars across 1229 unique pointings. The BGM significantly increases the number of stars considered above $\text{EIRP}_{\rm min} > 10^{15}$ W. We place limits on the prevalence of high-duty-cycle transmitters within 2.5 kpc, suggesting $\leq(0.000995 \pm 0.000002)$ per cent of stellar systems contain such a transmitter (for $\text{EIRP}_{\rm min} \gtrsim 5 \times 10^{16}$ W). This approach shows that single-dish surveys can place far stronger constraints on the prevalence of extraterrestrial transmitters across a wide diversity of stellar types. By incorporating this diversity through BGM simulations, we find that SETI surveys are, in fact, less biased by anthropocentric assumptions than often suggested.

We provide a calculator that enables users to identify the simulated stellar bycatch population for future single-dish SETI surveys. In addition, this approach is applicable to incoherent beamforming surveys [such as COSMIC (Commensal Open-Source Multimode Interferometric Cluster) on the VLA (Very Large Array) (C. D. Tremblay et al. 2025) or BLUSE (Breakthrough Listen's search for technosignatures using data from its User Supplied Equipment) on MeerKAT (D. Czech et al. 2021)] and interferometric SETI (such as

[1]The calculator code can be found at https://github.com/louisam11/SETI-Stellar-Bycatch-Simulator.

[2]Users are required to create an account to run BGM simulations, to enable access to the simulations through https://model.obs-besancon.fr/, as well as to receive an e-mail notification when the simulation is complete.

Table 2. An example output from the BGM, containing the first three stars simulated for pointing direction ($l = 0°$, $b = 30°$) and a field of view of 5 arcsec. Other user input values assume the use of the GBT *S*-band receiver for 5 min observations, with dechirping efficiency of 16.5 per cent and SNR of 10.

RA (°)	Dec. (°)	Dist (pc)	M_V	m_G	$G - V$	Age (10^9 yr)	Mass ($M_\odot$)	$T_{\rm eff}$ (K)	Spectral class	Luminosity class	$\mathrm{EIRP_{min}}$ (W)	$\mathrm{EIRP_{min,smear}}$ (W)
240.6209	−10.9977	314.1	10.44	18.84	0.830	3.958	0.499	3516	M2	Main sequence	2.318×10^{14}	1.405×10^{15}
240.6317	−10.9924	347.1	17.70	25.54	0.037	9.961	0.577	2324	WD DB	White dwarfs	2.830×10^{14}	1.715×10^{15}
240.6674	−10.9944	362.0	6.42	14.58	0.242	1.434	0.751	4687	K2	Main sequence	3.088×10^{14}	1.872×10^{15}
⋮			⋮				⋮				⋮	

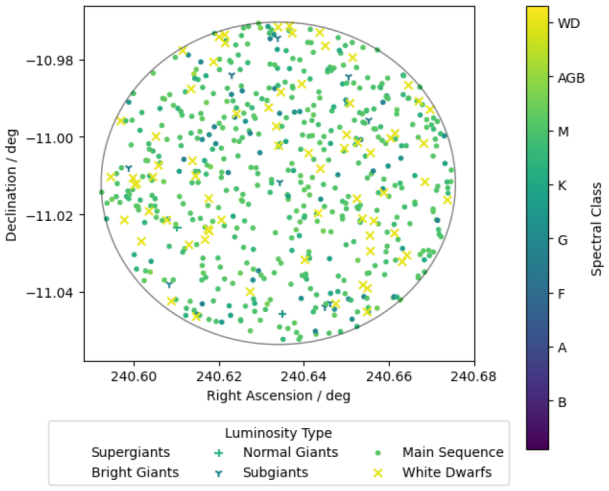

Figure 7. A demonstration of a typical field-of-view plot, produced by the calculator for a stellar bycatch sample captured within a 5 arcmin field of view, in the direction of ($l = 0°$, $b = 30°$). The diversity in spectral classes (colour-coded) and luminosity types (differentiated by marker) has been highlighted. Note that no supergiants or bright giants were found within this particular pointing.

K. Wandia et al. 2023; L. A. Mason et al. 2025). Incorporating more realistic constraints on the prevalence of extraterrestrial life promotes best practice in quantifying the true extent of SETI's uncharted parameter space and will help inform the design and interpretation of future surveys.

ACKNOWLEDGEMENTS

We would like to thank Dr Eamonn Kerins for invaluable discussion, as well as assistance from the BGM team (in particular Dr Céline Reylé) with the application of the BGM. The calculator utilizes code written by Raphael Meloir to launch simulations for the BGM web service and Gravpot web service. This work presents results from the European Space Agency (ESA) space mission *Gaia*. *Gaia* data are being processed by the *Gaia* Data Processing and Analysis Consortium (DPAC). Funding for the DPAC is provided by national institutions, in particular the institutions participating in the *Gaia* MultiLateral Agreement (MLA). This research has made use of the VizieR catalogue access tool, CDS, Strasbourg, France (F. Ochsenbein, P. Bauer & J. Marcout 2000). This work made use of ASTROPY, a community-developed core PYTHON package and an ecosystem of tools and resources for astronomy (Astropy Collaboration 2013, 2018, 2022).

DATA AVAILABILITY

This work presents results from the European Space Agency (ESA) space mission *Gaia*. The *Gaia* mission website is https://www.cosmos.esa.int/gaia. The *Gaia* archive website is https://archives.esac.esa.int/gaia.

REFERENCES

Arenou F. et al., 2018, A&A, 616, A17
Astropy Collaboration, 2013, A&A, 558, A33
Astropy Collaboration, 2018, AJ, 156, 123
Astropy Collaboration, 2022, ApJ, 935, 167
Bailer-Jones C. A. L., Rybizki J., Fouesneau M., Demleitner M., Andrae R., 2021, AJ, 161, 147
Bienaymé O., Leca J., Robin A. C., 2018, A&A, 620, A103
Choza C. et al., 2024, AJ, 167, 10
Czech D. et al., 2021, PASP, 133, 064502
Czekaj M. A., Robin A. C., Figueras F., Luri X., Haywood M., 2014, A&A, 564, A102
Déforêt B., Montillaud J., Robin A. C., Marshall D. J., 2024, in Béthermin M., Baillié K., Lagarde N., Malzac J., Ouazzani R. M., Richard J., Venot O., Siebert A., eds, Proceedings of the Annual Meeting of the French Society of Astronomy and Astrophysics (SF2A-2024). Société Française d'Astronomie et d'Astrophysique (SF2A), Paris, p. 145
Einasto J., 1979, in Burton W. B., ed., Proc. IAU Symp. No. 84, The Large-Scale Characteristics of the Galaxy. Reidel, Dordrecht, p. 451
Enriquez J. E. et al., 2017, ApJ, 849, 104
Gaia Collaboration, 2023, A&A, 674, A1
Gajjar V. et al., 2021, AJ, 162, 33
Garrett M. A., Siemion A. P. V., 2023, MNRAS, 519, 4581
Gehrels N., 1986, ApJ, 303, 336
Haywood M., 1994, A&A, 282, 444
Isaacson H. et al., 2017, PASP, 129, 054501
Johnson O. A. et al., 2023, AJ, 166, 193
Luri X. et al., 2018, A&A, 616, A9
Margot J.-L. et al., 2021, AJ, 161, 55
Margot J.-L. et al., 2023, AJ, 166, 206
Marshall D. J., Robin A. C., Reylé C., Schultheis M., Picaud S., 2006, A&A, 453, 635
Mason L. A., Garrett M. A., Wandia K., Siemion A. P. V., 2025, MNRAS, 536, 2127
Ochsenbein F., Bauer P., Marcout J., 2000, A&AS, 143, 23
Price D. C. et al., 2020, AJ, 159, 86
Ravinet T., Lagarde N., Reylé C., Amard L., Van Grootel V., 2022, in Brun A. S., Bouvier J., Petit P., eds, The 21st Cambridge Workshop on Cool Stars, Stellar Systems, and the Sun (CS21). Zenodo. Available at: https://doi.org/10.5281/zenodo.7586227
Reylé C., Marshall D. J., Robin A. C., Schultheis M., 2009, A&A, 495, 819
Robin A. C., Reylé C., Derrière S., Picaud S., 2004, A&A, 416, 157
Robin A. C. et al., 2022, A&A, 667, A98
Specht D., Kerins E., Awiphan S., Robin A. C., 2020, MNRAS, 498, 2196
Tremblay C. D. et al., 2025, AJ, 169, 122
Wandia K. et al., 2023, MNRAS, 522, 3784

Wlodarczyk-Sroka B. S., Garrett M. A., Siemion A. P. V., 2020, MNRAS, 498, 5720
Wright J. T., Kanodia S., Lubar E., 2018, AJ, 156, 260

APPENDIX: PREVALENCE ESTIMATES BY SPECTRAL TYPE

We consider the spectral diversity for shells of increasing distance (up to 10 kpc) for 1229 pointings. The prevalence is estimated for spectral shells where $N_* \geq 50$, given that the uncertainty in the number of stars is $\sqrt{N_*}$. Through the use of BGM simulations, we consider a broader range of potential sources for high-duty-cycle technosignatures when estimating the bycatch population.

Table A1. We estimate the prevalence of ETI transmitters, p, for shells of individual spectral classifications and distances ≤10 kpc, where $N_* \geq 50$.

		500 pc		1 kpc		5 kpc		10 kpc	
Type	Class	N_*	p (per cent)	N_*	p (per cent)	N_*	p (per cent)	N_*	p (per cent)
Bright giants	G	0	–	0	–	16	–	60	$<5.0 \pm 0.6$
	K	0	–	1	–	25	–	57	$<5.3 \pm 0.7$
Normal giants	A	0	–	6	–	124	$<2.4 \pm 0.2$	403	$<0.74 \pm 0.04$
	F	0	–	10	–	216	$<1.4 \pm 0.1$	669	$<0.45 \pm 0.01$
	G	5	–	67	$<4.5 \pm 0.5$	2035	$<0.147 \pm 0.003$	8308	$<0.036 \pm 0.001$
	K	3	–	80	$<3.8 \pm 0.4$	2362	$<0.127 \pm 0.003$	7561	$<0.040 \pm 0.001$
	M	0	–	6	–	88	$<3.4 \pm 0.4$	308	$<0.97 \pm 0.06$
Subgiants	B	0	–	0	–	39	–	106	$<2.8 \pm 0.3$
	A	0	–	10	–	242	$<1.2 \pm 0.1$	727	$<0.41 \pm 0.02$
	F	23	–	305	$<0.98 \pm 0.06$	10 169	$<0.030 \pm 0.0003$	41 058	$<0.007 \pm 4 \times 10^{-5}$
	G	6	–	82	$<3.7 \pm 0.4$	2291	$<0.131 \pm 0.003$	7101	$<0.042 \pm 0.0005$
Main sequence	B	0	–	3	–	91	$<3.3 \pm 0.3$	315	$<0.95 \pm 0.05$
	A	1	–	25	–	657	$<0.46 \pm 0.02$	2044	$<0.147 \pm 0.003$
	F	69	$<4.3 \pm 0.5$	585	$<0.51 \pm 0.02$	19 179	$<0.016 \pm 0.0001$	75 744	$<0.004 \pm 1 \times 10^{-5}$
	G	257	$<1.2 \pm 0.1$	1768	$<0.170 \pm 0.004$	54 715	$<0.005 \pm 2 \times 10^{-5}$	207 808	$<0.001 \pm 3 \times 10^{-6}$
	K	611	$<0.49 \pm 0.02$	4258	$<0.070 \pm 0.001$	125 692	$<0.002 \pm 7 \times 10^{-6}$	501 400	$<0.0005 \pm 8 \times 10^{-7}$
	M	6059	$<0.050 \pm 0.001$	32 328	$<0.009 \pm 5 \times 10^{-5}$	820 425	$<0.0004 \pm 4 \times 10^{-7}$	2696 160	$<0.0001 \pm 7 \times 10^{-8}$
	AGB	251	$<1.2 \pm 0.1$	1316	$<0.23 \pm 0.01$	28 453	$<0.011 \pm 6 \times 10^{-5}$	81 198	$<0.004 \pm 1 \times 10^{-5}$
White dwarfs	DA	310	$<0.97 \pm 0.06$	2302	$<0.130 \pm 0.003$	92 980	$<0.003 \pm 1 \times 10^{-5}$	442 050	$<0.0007 \pm 1 \times 10^{-6}$
	DB	236	$<1.3 \pm 0.1$	1381	$<0.22 \pm 0.01$	32 809	$<0.009 \pm 5 \times 10^{-5}$	92 144	$<0.003 \pm 1 \times 10^{-5}$
	DC	235	$<1.3 \pm 0.1$	1412	$<0.21 \pm 0.01$	32 711	$<0.009 \pm 5 \times 10^{-5}$	91 644	$<0.003 \pm 1 \times 10^{-5}$

This paper has been typeset from a TEX/LATEX file prepared by the author.